Desalination and Water Treatment
www.deswater.com

doi: 10.5004/dwt.2021.26456

210 (2021) 402–414
January

$FeNi_3$@SiO_2@CuS magnetic nanocomposite: synthesizing, characterization, and application for methylene blue adsorption

Negin Nasseh[a], Tariq J. Al-Musawi[b], Rasoul Khosravi[a], Ayat Hossein Panahi[c], Fatemeh Sadat Arghavan[d], Behnam Barikbin[a,e,*]

[a]*Department of Environmental Health Engineering, Faculty of Health, Social Determinants of Health Research Center, Birjand University of Medical Sciences, Birjand, Iran, emails: B_Barikbin@yahoo.com (B. Barikbin), negin_nasseh@yahoo.com (N. Nasseh), khosravi.r89@gmail.com (R. Khosravi)*
[b]*Department of Civil Engineering, Faculty of Engineering, Isra University, Amman, Jordan, email: tariq.almusawi@iu.edu.jo (T.J. Al-Musawi)*
[c]*Social Determinants of Health Research Center, Birjand University of Medical Sciences, Birjand, Iran, email: ayatpanahi@yahoo.com (A. Hossein Panahi)*
[d]*Student Research Committee, Department of Environmental Health Engineering, Faculty of Health, Mashhad University of Medical Sciences, Mashhad, Iran, email: fatemeh.arghavan71@gmail.com (F.S. Arghavan)*
[e]*Social Determinants of Health Research Center, Mashhad University of Medical Sciences, Mashhad, Iran*

Received 31 December 2019; Accepted 12 August 2020

ABSTRACT

A novel magnetic nanocomposite adsorbent formed from the coating $FeNi_3$ nanoparticles with SiO_2 nanoparticles, and then with CuS nanoparticles ($FeNi_3$@SiO_2@CuS) was successfully synthesized and then applied, for the first time, for eradicating methylene blue (MB) dye-laden wastewater. An adsorptive performance test were conducted using a batch system with variations of several water quality parameters, including pH, contact time, MB concentration, $FeNi_3$@SiO_2@CuS dose, and competitor NaCl concentration. The characterization study using transmission electron microscopy, field emission scanning electron microscopy, and vibrating sample magnetometer approaches demonstrated that $FeNi_3$@SiO_2@CuS has a number of favorable morphological, physiochemical, and adsorptive properties which make it a potential adsorbent toward organic pollutants. The equilibrium analysis of non-linear fit method revealed that the Langmuir equation was the best model for the representation of isothermal data, where the maximum uptake reached 24.457 mg/g. The kinetic adsorption behavior of methylene blue on $FeNi_3$@SiO_2@CuS obeyed the pseudo-second-order kinetics. The nature of the adsorption was also endothermic and spontaneous, as the thermodynamic study revealed. During the adsorption experiments, $FeNi_3$@SiO_2@CuS magnetic nanocomposite exhibited an excellent adsorption capacity toward MB molecules, where the maximum removal efficiency of 85.21% was recorded at pH = 12, contact time = 180 min, initial MB concentration = 20 mg/L, and $FeNi_3$@SiO_2@CuS dose = 2 g/L. It was also found that NaCl presence had a negative impact on that efficiency. The mechanism of MB interaction with $FeNi_3$@SiO_2@CuS involved both chemical and physical adsorption processes. Results of this study unraveled that the adsorption process using $FeNi_3$@SiO_2@CuS as an adsorptive agent could be a promising treatment technology for the removal of MB dye from high alkaline wastewater.

Keywords: $FeNi_3$@SiO_2@CuS; Magnetic nanocomposite; Methylene blue; Adsorption; Characterization

* Corresponding author.

1. Introduction

The world, at the present time, faces great challenges in the fields of water quality, management, and environmental pollution, due to the discharge of highly polluted liquid wastes into the aquatic environment [1]. Generally, to pass these challenges, there is an incessant search for developing innovative and high-performance technologies to purify wastewater prior to discharge into receiving water bodies. In addition, the increasing rate in industrialization in the last three decades had exacerbated environmental problems resulting from pumping industrial effluents-containing contaminants into water resources [2]. In fact, the untreated or ineffectively treated wastewater often carries high concentrations of substances that damage the total environment and humans. For example, it was found that approximately 22% of the total quantity of used raw dyes was released in an improperly or inadequately treated wastewater from various industrial processes such as painting; printing and plastics; leather and tannery; textiles, cosmetics, and food processing [3]. Therefore, the discharge of industrial wastewater containing contaminants, like dyes to the sewer system, is forbidden in several countries unless such contaminants are reduced, at their generation source, to the permissible concentrations [4].

Methylene blue dye (MB) is a basic, cationic, photoactive, and azo dye. Its commercial form is currently used in many industrial, pharmaceutical, and medical applications [5]. The textile and clothing industries are the largest consumer industries that use MB for dyeing wool, linen, cotton, and silk fabrics. In addition, MB dye has medical uses such as treatment of methemoglobinemia and Alzheimer diseases, and to detect fistula in surgery [6]. Its oral form is used in dentistry to diagnose areas with plaque microbial teeth. Table 1 lists more details about the chemical and physical properties of MB dye. Although, MB dye has beneficial uses and is normally not considered as a hazardous element yet, it can cause complications such as eye burns, stomach, intestines, and skin irritation [5]. Excessive exposure to this dye may also lead to problems with breathing, jaundice, tissue necrosis, nausea, vomiting, severe sweating, cyanosis, mental disorder, cardiovascular disorders such as hypertension, dizziness, fever, headache, and anemia. In addition, the presence of dyes in the river or other surface water bodies can cause several adverse effects on the aquatic environment. For example, it might create unpleasant color, impede sunlight penetration into the water body thus impairing the essential photosynthesis process by the aquatic plants, which leads to eutrophication (rapid and excessive growth of algae), and increase water hardness and turbidity. All these effects lead to disturbance and sometimes to death because of organisms living in the receiving water [7]. In consequence, dyes removal from wastewater prior to pumping to aquatic systems is an extremely important requirement for protecting humans and the environment from pollution, and an issue that attracted great attention from ecologists and scientists [8,9].

Adsorption process is a superior, easy, efficient, cost-effective, and thus widely used purification technology for removing various hazardous elements and compounds from wastewater [6,10]. This treatment method involves using a solid material, called "adsorbent", that has an ability to remove harmful materials; called "adsorbate" from aqueous solution [11]. However, the selected adsorbents should be intensively tested, before being applied, for their adsorption ability toward target adsorbate. After the invention of adsorbents of nanoscale particles, new horizons in the adsorption treatment methods have been opened [12]. In particular, the magnetic nanoparticles such as $FeNi_3$, has been recommended by a number of studies to be applied as adsorbents in the adsorption treatment system [13]. This is because these particles have several adsorptive characteristics and operation properties. Most importantly, magnetic nanoparticles can be easily withdrawn from the solutions using a magnet. Thus, they do not need an additional method like nanofiltration to separate them from the treated water [14,15]. It is noteworthy that the magnetic nanoparticles in nature have a high orientation to agglomerate as a result of the high magnetite properties of their large surface area [16]. Therefore, modifying the surface of nanoparticles, by coating using organic materials or minerals to prevent the attraction among the magnetite particles, is an essential approach to overcome the above-mentioned problem associated with their agglomeration in the adsorption system. In a few recent years, it has been found that numerous nanocomposites have been applied to coat the surface of the magnetic particles. Due to their excellent properties such as simplicity in preparation, low cost, good compatibility with other chemicals, and high stability in different environmental parameters, silica is found to be an appropriate material for coating $FeNi_3$ nanoparticles. In fact, SiO_2 forms a shell around the $FeNi_3$ nanoparticle (nucleus) reducing attraction among $FeNi_3$ nanoparticles, which in turn, facilities their dispersion. The dispersion of adsorbent particles in the aqueous solution is an important point that should be accomplished in order to spread these particles during the synthesizing or adsorption process, thus achieve maximum benefits from the synthesized particles [17–19]. Moreover, Copper sulfide (CuS) particles, have recently attracted several researchers to be used in the treatment processes because of their brilliant practical physical and chemical properties. Particles of this compound also have a magnetic property that facilitates separating them from the aqueous solution by the magnet. Accordingly, we suppose that the combined particles of $FeNi_3$, SiO_2, and CuS to form $FeNi_3$@SiO_2@CuS can be presented as an effective material for removing contaminants in the adsorption units [20]. To the knowledge of researchers, few works have examined the adsorptive performance of $FeNi_3$@SiO_2@CuS regarding eliminating MB dye from wastewater. Therefore, the principal objectives of this work are (i) to prepare and characterize $FeNi_3$@SiO_2@CuS magnetic nanocomposite, (ii) to investigate the effects of some water quality parameters including NaCl concentration on the performance of $FeNi_3$@SiO_2@CuS for MB adsorption, and (iii) to discuss, in detail, the isotherm, kinetics, and thermodynamic adsorption of MB molecules onto $FeNi_3$@SiO_2@CuS magnetic nanocomposite.

2. Materials and methods

2.1. Chemicals and reagents

The working solutions of MB dye were prepared by diluting high purity (99.9%) stock solution of concentration = 100 mg/L. Polyethylene glycol (PEG, molecular

weight = 6,000 g/mol), iron(II) chloride ($FeCl_2(4H_2O)$), copper sulfate ($CuSO_4$), nickel chloride ($NiCl_2(6H_2O)$), ethylene glycol ($C_2H_6O_2$), hydrazine hydrate ($N_2H_4{\cdot}H_2O$, purity = 80%), tetraethyl ortho silicate ($SiC_8H_{20}O_4$), ethanol, ammonia, and sodium thiosulfate ($Na_2S_2O_3$) solutions were used in synthesizing and preparing of $FeNi_3@SiO_2@CuS$. The effect of competitor salt, that is, NaCl on adsorption process was also detected. The above-mentioned chemicals are of an analytical grade; where they were used as purchased from the manufacturer (Merck, Germany). HCl and NaOH solutions (0.1 N) were also prepared in the laboratory and used during the adsorption experiments to control pH level of MB solutions using Knick-765Caliamatic pH meter.

2.2. Synthesizing and preparing of $FeNi_3@SiO_2@CuS$

The process of synthesizing $FeNi_3@SiO_2@CuS$ and preparing it as an adsorbent, are summarized in the following steps. Notably, all the materials were prepared using glass flasks of 500 mL. Initially, 1 g of PEG was completely dissolved by vigorous stirring with deionized water (200 mL) and poured into a flask. Then, two separate solutions were prepared from dissolving 0.6 g of $FeCl_2{\cdot}4H_2O$ and 1.4 g of $NiCl_2{\cdot}6H_2O$ in 30 mL of deionized water then simultaneously added to the contents of the flask. Afterwards, 27 mL of $N_2H_4{\cdot}H_2O$ was introduced to the prepared suspension which was vigorously stirred for 24 h. Notably, the pH of this suspension was stabilized at value 13 by drop-wise addition of NaOH during mixing time. The mixture is left to settle down, where the black precipitate represents the $FeNi_3$ nanoparticles. These nanoparticles were withdrawn using an N_{42} magnet, washed until the decanted water becomes close to neutral pH, then oven-dried at 80°C to ensure dryness [21].

The obtained $FeNi_3$ nanoparticles were covered by SiO_2 adopting the following steps [22]. A homogenous solution of 2 mL of ammonia, 80 mL of ethanol, and 20 mL of deionized water, was prepared in the laboratory. A 0.5 g of $FeNi_3$ nanoparticles was added to the solution, and the nanoparticles were dispersed using Intellect FR USC 22 LQ ultrasonic cleaning equipment (Germany). Then, 1 mL of $SiC_8H_{20}O_4$ was added to the previous solution through dripping then stirred for 24 h at 400 rpm. At the moment, the $FeNi_3@SiO_2$ magnetic nanoparticles were formed. These nanoparticles were then separated from the solution, washed gently with ethanol than with deionized water, till completely dried at up 60°C.

Ultimately, to get the final product of $FeNi_3@SiO_2@CuS$, a quantity of $FeNi_3@SiO_2$ nanoparticles (≈0.15 g) was dispersed for a period of 30 min in 20 mL of ethylene glycol. Subsequently, the dispersed material was poured into a flask which was placed in an oil bath device where the oil temperature was maintained at 120°C. Afterwards, about 0.8 g of $CuSO_4$ compound was added to the flask's content and shaken at 300 rpm for 24 h. Then, 1.9 g of $Na_2S_2O_3$ was dispersed in 20 mL ethylene glycol and further added to flask content. The mixture was refluxed at 140°C for 90 min, then left to cool [20]. The solid product (called: $FeNi_3@SiO_2@$ CuS magnetic nanocomposite) was separated by a magnet, washed, dried at 80°C for 5 h, and finally stored in a stopper glass flask for use in the subsequent analysis.

2.3. Characterization analysis

Depiction devices of TEM (ZEISS Sigma, EM10C-100 KV, Germany) and FESEM (ZEISS Sigma, VP-500, Germany) were used to capture high-resolution microscopic images for the synthesized nanocomposite. These images are very helpful in detecting surface morphology and appearance of the synthesized adsorbent. In addition, the magnetism force of the synthesized adsorbent nanoparticles was measured based on VSM analysis using Lake Shore-7400 magnetometer (USA). The FTIR analysis of the synthesized nanocomposite prior to and after MB adsorption was conducted at wave number range: 400–4,000 cm^{-1} using Perkin Elmer (Waltham, MA 02451 USA)-spectrum 65 spectroscopy (USA). In fact, this analysis is essential to detect the active groups of the used adsorbents. To determine the important characterization parameter, that is, pH_{pzc} of the used adsorbent, each of the nine flasks was filled with 50 mL of deionized water, where the initial pH values were separately adjusted to 2, 4, 6, 8, and 10. Next, 0.2 g of the synthesized nanocomposite was introduced into each flask, then shaking them at 300 rpm for 24 h using a shaker; the final pH of each supernatant was measured. Initial and final pH data were plotted in one graph; where pH_{pzc} value represents the intercept point between the two plots.

2.4. Experimental work

The experiments of MB adsorption onto $FeNi_3@SiO_2@$ CuS magnetic nanocomposite were done in several batches in dark conditions. The MB removal efficiency was examined for various experimental conditions: pH (2–12), $FeNi_3@$ $SiO_2@CuS$ magnetic nanocomposite dose (0.2–2 g/L), initial MB concentration (10–60 mg/L), contact time (0–180 minutes), and solution temperature (5°C–50°C). In addition, the effect of NaCl concentration presented in the MB solution on this dye removal efficiency was determined in the present study. Therefore, five flasks with 100 mL of 20 mg/L MB and 0.2 g $FeNi_3@SiO_2@CuS$ magnetic nanocomposite were prepared in the laboratory. Next, NaCl salt of 0.5, 0.1, 0.05, 0.01, and 0.001 M concentration were adjusted in the prepared solutions. The flasks were shaken for 60 min at 300 rpm at ambient temperature. Afterwards, the samples were withdrawn and tested for their remaining MB concentration.

At a specific adsorption time interval, 3 mL aqueous samples were sucked up from each flask using a syringe, then filtered by using Whatman filter papers, and centrifuged. Afterwards, the supernatant solution was tested for the residual concentration of MB using T80 UV-vis double-beam spectrophotometer (UK), where the device was fixed at a wave length peak of 665 nm [23]. To ensure accurate results, the MB concentration in each sample was analyzed twice and the averaged values were calculated. The adsorption uptake (q_e, mg/g) and the removal efficiency (RE%) were calculated as follows [24]:

$$q_e = \left(\frac{C_e - C_0}{M}\right) \times V \tag{1}$$

$$\mathrm{RE}\% = \left(1 - \frac{C_e}{C_0}\right) \times 100 \tag{2}$$

where C_0 and C_e are the measured MB concentrations (mg/L) before and after specific time of adsorption, respectively; M denotes the $FeNi_3@SiO_2@CuS$ magnetic nanocomposite mass (g), and V is the volume of MB solution used in experiment = 0.1 L.

It is worth noting that the thermodynamic; isotherm, and kinetic adsorption processes were analyzed based on the results of effects of temperature; adsorbent dose, and reaction time, respectively.

2.5. Isotherm, kinetics, and thermodynamics studies

To comply with isotherm data, three formulas were selected: Langmuir; Freundlich, and Temkin. These isotherm formulas are widely applied in the literature by many researchers to describe the type of adsorption of various pollutants onto different adsorbents. The Langmuir equation is a widely used isotherm model for describing the mono-layer sorption interaction between the pollutant molecule and homogeneous sites over the adsorbent used. This model can be mathematically represented as shown in Eq. (3) [25,26].

$$q_e = \frac{q_{\max} K_L C_e}{1 + K_L C_e} \tag{3}$$

where $q_{\max}$ represents the maximum uptake of pollutant molecules by the adsorbent (mg/g), and K_L is the constant that reflects the affinity level of the active sites of the adsorbent for adsorption of pollutant molecules at the equilibrium condition (L/mg).

The basic characteristic of the non-dimensional constant of the Langmuir equation is called the dimensionless separation factor (R_L) as Eq. (4), where the favorable adsorption case of pollutant molecules onto the adsorbent particles takes place at the values of $0 < R_L < 1$ [27].

$$R_L = \frac{1}{\left(1 + K_L C_0\right)} \tag{4}$$

Freundlich isotherm model is an empirical equation (Eq. (5)). Unlike the Langmuir model, this model proposes that the adsorbent surface comprises heterogeneous and multi-layered active sites.

$$q_e = K_F C_e^{\frac{1}{n}} \tag{5}$$

where n is an empirical parameter of the Freundlich equation (g/L) represents system heterogeneity, and K_F is adsorption capacity constant (mg/g). In addition, the desirability of the adsorption process can be determined if $1/n$ was <1.

Temkin model is a complex isotherm one that describes indirect interactions between pollutant molecules and adsorption sites in the liquid–solid adsorption system. If the Temkin model was applicable to the adsorption process, then the heat of adsorption of target pollutant molecules onto the layer of adsorbent's sites would linearly decrease in accordance with the increase of surface coverage. It was found that this model is perfect to be applied to intermediate pollutant concentrations [28,29].

$$q_e = B \frac{RT}{B_t} \ln\left(A_t C_e\right) \tag{6}$$

where A_t is a constant of Temkin model that denotes equilibrium binding (L/g); B_t is adsorption heat constant (J/mol); R is the constant of universal gas (8.314 J/mol K), and T is the thermodynamic temperature (K).

The modeling of the experimental data of the pollutant kinetic mechanism with the appropriate mathematical models, is a necessary step to ensure a successful design of the treatment adsorption unit. Until recently, the well-known kinetic equations of pseudo-first-order (Eq. (7)) and pseudo-second-order (Eq. (8)) have been widely made used of in the literature to describe that field [30]. Each of these two kinetic formulas expresses the kinetic adsorption in different mechanisms, that is, physical or chemical adsorption [31]. Besides these kinetic models, Elovich model (Eq. (9)) has become an increasing application in adsorption studies [32,33].

$$q_t = q_e\left(1 - e^{-k_1 t}\right) \tag{7}$$

$$q_t = \frac{k_2 q_e^2 t}{1 + k_2 q_e t} \tag{8}$$

$$q_t = \frac{1}{\beta} \ln\left(1 + \alpha\beta t\right) \tag{9}$$

where q_t stands for the adsorption uptake (mg/g) calculated at a specific time of adsorption process (t, min); k_1 and k_2 represent constants of reaction rate (1/min) of the first- and second-order kinetic rate, consecutively, and α and β are the constants of Elovich equation.

Eventually, Gibbs free energy change ($\Delta G°$, kJ/mol); entropy ($\Delta S°$, kJ/mol K); and enthalpy ($\Delta H°$, kJ/mol) parameters, associated with the thermodynamic of MB adsorption onto $FeNi_3@SiO_2@CuS$ magnetic nanocomposites, were elicited from results of effects of temperature through using Eqs. (10)–(12) [22,34–36].

$$\Delta G° = -RT \ln K_d \tag{10}$$

$$\ln K_d = -\frac{\Delta H°}{RT} + \frac{\Delta S°}{R} \tag{11}$$

With

$$K_d = \frac{q_e}{C_e} \tag{12}$$

where K_d denotes equilibrium constant (L/g).

The compatibility of experimental data with mathematical models was done by nonlinear regression methods. In this

study, the best model was chosen, in this study, based on the results of the two statistical parameters: correlation coefficient results (R^2), and root mean square error (RMSE). In this context, high R^2 and small RMSE values denote high compatibility between the applied model and the experimental data.

3. Results and discussion

3.1. Characterization study

All results of characterization analyses by means of field emission scanning electron microscopy (FESEM), transmission electron microscopy (TEM), vibrating sample magnetometer (VSM), and Fourier transform infrared (FTIR) are presented in Fig. 1. FESEM micrograph captured at magnification of 20 KX (Fig. 1a) indicates that $FeNi_3$@SiO_2@CuS surface is rugged and coarse in nature. In addition, it appeared that this adsorbent consists of several spherical and highly agglomerated aggregates of nano size, with the approximate diameter range of 24–63 nm. The property of agglomeration is caused by high magnetic force of the synthesized $FeNi_3$@SiO_2@CuS nanoparticles, leading to coalescence among these particles. The $FeNi_3$@SiO_2@CuS adsorbent can also be characterized by a porous material, due to its possessing of a large number of small pores and cavities. These properties provide a high specific area for reaction and adherence to the pollutant molecules. These findings present the adsorbent, under investigation in the present study, as a superior material that can be effectively used in adsorption systems.

The high-resolution TEM image of the $FeNi_3$@SiO_2@CuS particle is displayed in Fig. 1b. The synthesized nanoparticles are amorphous with asymmetrical shape. It is apparent that the synthesized nanoparticles of this adsorbent are multidispersed, so the agglomeration of them was high.

Furthermore, magnetism property of the synthesized adsorbent was also determined through VSM analysis. In fact, nanoparticles of low magnetic value that applied

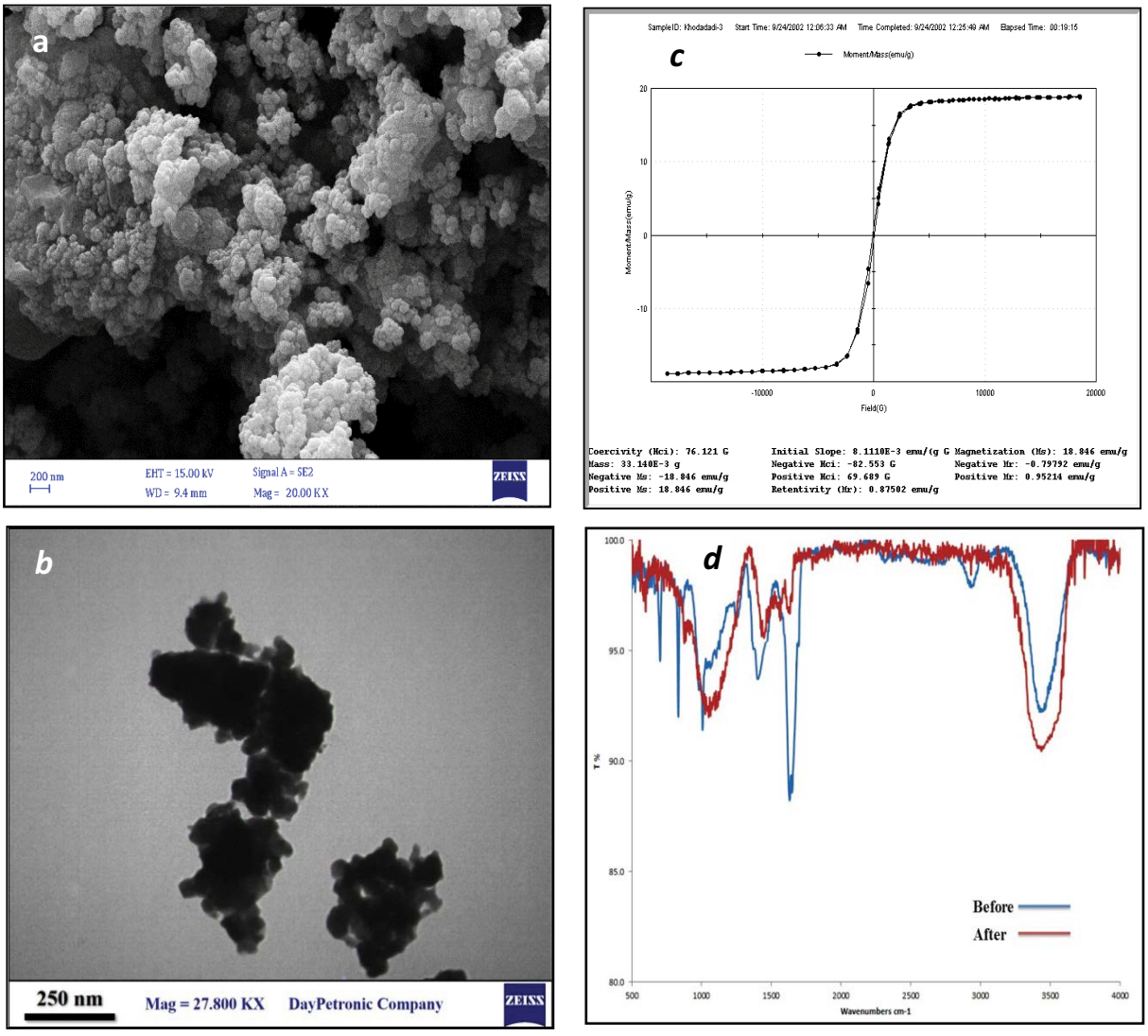

Fig. 1. SEM micrograph (a), TEM micrograph (b), VSM analysis (c), and FTIR spectra (d) of $FeNi_3$@SiO_2@CuS magnetic nanocomposite.

in water treatment methods require advanced separation methods in order to separate them from the treated solutions which are unfavorable in several applications as they add more costs to the treatment system. The obtained hysteresis loop of the magnetization curve (Fig. 1c), indicates that the $FeNi_3@SiO_2@CuS$ particles have a high magnetic property as their saturation magnetization values are found to be 18.72 emu/g. Thus, $FeNi_3@SiO_2@CuS$ magnetic nanocomposite can be, after adsorption, easily isolated from solutions via a magnetic field, without further need for advanced separation technology like nanofiltration [37].

The XRD patterns of the $FeNi_3@SiO_2@CuS$ magnetic nanocomposite with its parent particles (FNSCS) are presented in Fig. 2a. The peaks detected at 75.47°, 51.18°, and 44.24° reflect the presence of $FeNi_3$ nanoparticles in the structure of the prepared adsorbent (JCPDS card no. 38-0419). The wide peak of 2θ = 10°–25° was also related to the amorphous silica (JCPDS card No. 29-0085), ascertaining the presence of a silica layer in the nanoparticles. The peaks detected at 2θ = 29.35°, 31.85°, 32.13°, 48.04°, 52.69°, and 59.38° are related to the presence of CuS compound (JCPDS Card No. 06-0462). The size of each nanoparticle was calculated using the Debye–Scherrer equation (Eq. (13)), amounted to 48 nm confirming nano size range of the used adsorbent.

$$D = \frac{0.98\lambda}{\beta\cos\theta} \tag{13}$$

where D is the diameter of nanoparticle (nm), θ is the diffraction angle in the peak (radians), β is the peak width in half-length (radian) located at 2θ in the obtained XRD pattern, and λ is the wavelength of the applied X-ray which is equal to 0.1540 nm.

The EDS pattern of $FeNi_3@SiO_2@CuS$ magnetic nanocomposite is presented in Fig. 2b. The formation of the $FeNi_3$ magnetic nanoparticles (core) of used adsorbent can be clearly deduced, due to the atomic Fe to Ni ratio, which is approximately 1:3. The peak detected at 1.8 keV relates to the low constituent of silica in the structure of $FeNi_3@SiO_2@CuS$. In addition, copper presence with a high ratio confirms the element as CuS (outer layer) onto $FeNi_3@SiO_2@CuS$ magnetic nanocomposite.

To identify type of the functional groups, responsible for MB adsorption, FTIR spectra of $FeNi_3@SiO_2@CuS$ magnetic nanocomposite samples prior to and after MB adsorption were carried out (Fig. 1d). For FT-IR spectrum prior to MB adsorption, the blue curve in Fig. 1d, vibration of Ni and Fe metals during the nanocomposite synthesis is the reason behind emergence of Fe–Ni–Ni, Ni–Fe–Ni, and Fe–Ni–Ni groups below 600 cm^{-1}. Owing to the presence of SiO_2 for nanocomposite synthesis, the sharp peaks detected at 808 and 1,100 cm^{-1} correspond to the extended vibration of the Si–OH, Si–O–, Si–O–Si groups [13,38]. The vibration peaks belonging to the SiO_2 group are appropriated to asymmetric and symmetric tensile modes. The 3,440 cm^{-1} broad peak corresponds to OH^- stretching vibration caused by the presence of water in the structure of the synthesized nanocomposite [39]. The peak at 1,639 cm^{-1} relates to H–OH of SiO_2 [40]. These peaks confirm that SiO_2 is well coated on the surface of $FeNi_3$ nanoparticles. The sharp peak observed

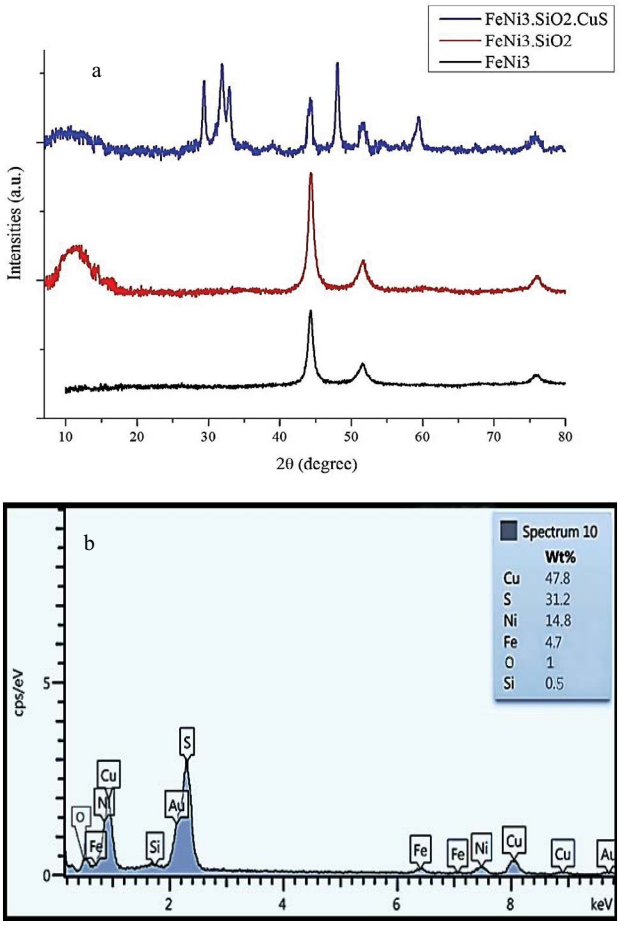

Fig. 2. XRD patterns of $FeNi_3@SiO_2@CuS$, $FeNi_3@SiO_2$, and $FeNi_3$ (a), and EDS pattern of $FeNi_3@SiO_2@CuS$ (b).

in the range of 887.75 cm^{-1} may correspond to the vibration of Ni–Cu, Fe–Cu, and Fe–Ni–Cu bonds. The weak peaks ranging from 1,010 to 1,030 cm^{-1} can be attributed to Ni–SiO_2 and Fe–SiO_2 bonds. The 1,356.19 cm^{-1} peak refers to the C–H and N–O groups that confirm presence of polyethylene glycol or hydrazine hydrate as residuals of raw materials in the structure of synthesized nanocomposite [13,41]. After MB adsorption (red curve in Fig. 1d), resulting from the reaction between MB molecules and active groups of the nanocomposite, some peaks intensity moved to new values. According to the curve, it is obvious that there are transformations in peak intensity at 3,400; 1,100; and 1,356 cm^{-1} wavelength associated with the interaction of MB molecules with the O–H, Si–O–, and C–H bonds in the synthesized nanocomposite, respectively.

3.2. pH effects

A number of studies demonstrated that pH of the aqueous solution can affect the efficiency degree of adsorption process through several mechanisms. Generally, at different pHs the adsorbate or pollutant molecules may have different surface charges. On the other hand, the surface properties or the degree of ionization of the used adsorbent

greatly depend on pH value [42]. Therefore, the determination of pH_{pzc} value of the used adsorbent is very important to make in order to indicate the condition at which the net charge of the functional groups existing on the adsorbent surface is neutral [43]. According to the conducted analysis, the pH_{pzc} of the $FeNi_3@SiO_2@CuS$ magnetic nanocomposite was determined to be 6.18 (Fig. 3a), therefore, the surface charge of the $FeNi_3@SiO_2@CuS$ magnetic nanocomposite will be negative when this adsorbent is presented in a solution of pH > 6 and vice versa. However, the current study investigated the pH influence of the MB dye solution on the removal efficiency of this dye via $FeNi_3@SiO_2@CuS$ magnetic nanocomposite within the range of 2–12 (Fig. 3b). The results of this figure revealed that MB dye removal percentage increased in ratio to the increase of pH values. This phenomenon can be illustrated in light of both pH_{zpc} value of the adsorbent and pk_a value of the adsorbate. These values indicated that the dominating charge of $FeNi_3@SiO_2@$ CuS nanoparticle is positive in the pH value < 7, in addition, the MB is characterized by being cationic dye in the acidic medium as its pk_a value = 3.8 (Table 1). All these factors contribute to an increase in the electrostatic repulsion forces of the cationic MB molecules and adsorbent particles of positive charges. Therefore, the removal efficiency of the MB will be low as the number of negative reaction sites on $FeNi_3@SiO_2@CuS$ nanoparticles has been limited to the acidic pH values. Furthermore, it is well known that the H^+ protons are more concentrated in acidic values which might jostle the cationic dye molecules to be adsorbed onto negative charge sites of the used adsorbent [42,44]. It is worth to mention that these protons are responsible for reacting with the dye anions in the aqueous solution at pH < pk_a, such a reaction will lead to present dye molecules of neutral charge. In this way, the dye molecules will remain trapped in water solution without any reaction with the adsorbent particles. As the pH solution becomes above 6, the functional sites of the adsorbent gets negative charge in charge and that would be ideal attraction positions and adsorption sites for positively charged dye molecules [45]. In this case, the attraction force will increase through increasing the pH value, which in turn, increases the percentage of removal as results in Fig. 2 show. Notably, these results were found to be fully in compliance with these of both Liu et al. [11] and Coşkun et al. [46].

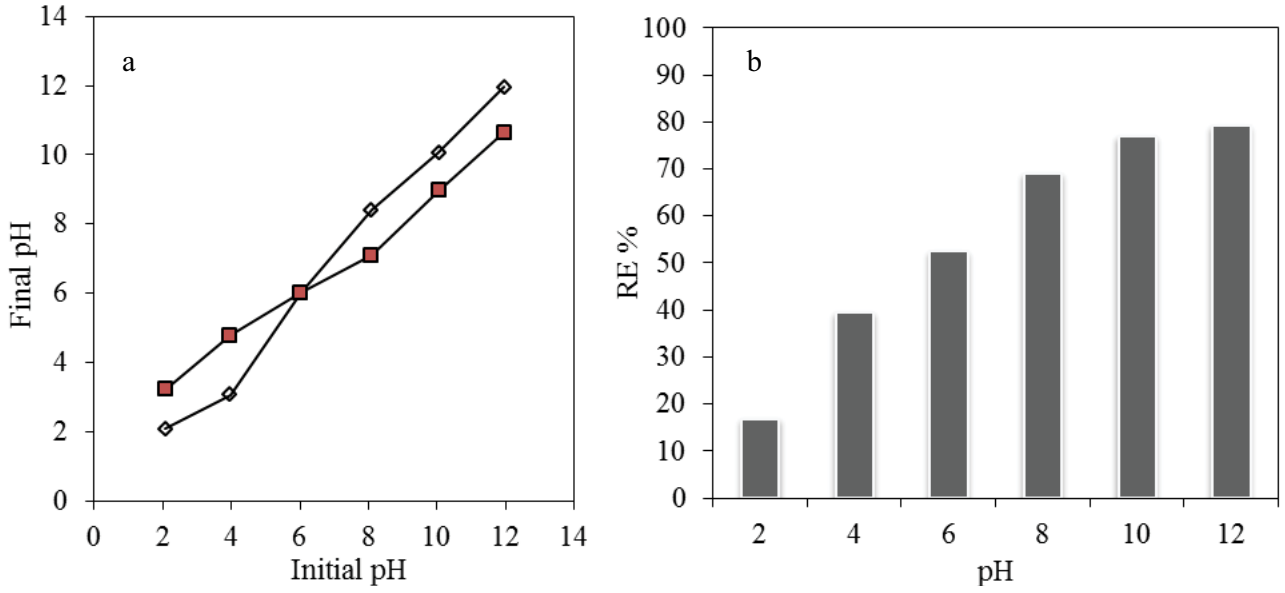

Fig. 3. Plots of results of the pH_{pzc} analysis (a), and effect of pH values on the adsorption process (b) ($FeNi_3@SiO_2@CuS$ dose = 1 g/L, initial dye concentration = 30 mg/L, contact time = 60 min, and temperature at ambient condition).

Table 1
Physicochemical properties of MB dye molecule

Formula	$C_{16}H_{18}N_3SCl$	Chemical structure
Molecular weight	319.85 g/mol	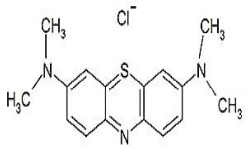
pk_a	3.8	
λ_{max}	665 nm	
Color	Blue	
Type	Cationic	
Name according to IUPAC rules	Bis(dimethylamino) phenotiazin e-5-ium-chloride	

3.3. Initial concentration and contact time effects

This study, impact of MB concentration on the adsorption process was tested in relation to different values (10, 20, 30, 40, 50, and 60 mg/L). The results of the experiment presented in Fig. 4 were plotted as a contact time function (0–180 min), where the pH and $FeNi_3$@SiO_2@CuS dose are fixed at values of 12 and 1 g/L respectively. It can be clearly noted that an increase in the initial concentration of MB negatively effects adsorption capacity of the adsorbent used reducing removal efficiencies. This is because the amount of adsorbent used in this test is the same for all applied MB concentrations, so the number of binding sites is also equal. Thus, as pollutant molecules concentration increases in the aqueous solution while the amount of adsorbent stays stable, that leads to an increase in the competitiveness between them on the specified sorption sites. This phenomenon was also presented in the same study that discussed MB removal from aqueous solution by using magnetic carbon nanotube [47]. Other brilliant results regarding the adsorption equilibrium are determined by this experimentation test. In this context, Fig. 4 reveals that the removal efficiencies at different initial MB concentration increased with prolonged contact time until they reached the equilibrium level within the first 60 min. In fact, one can conclude that the adsorption process was rapid as results indicated that more than half of the removal efficiency was achieved in the first 30 min of contact time [48,49]. The abundance of uncovered sorption sites which not occupied by contaminant molecules at the first stage of contact were behind this behavior. For practical application perspectives, the rapid pollutants removal of applied $FeNi_3$@SiO_2@CuS is considered as a positive property to such adsorbent to be a good media for treatment processes. The studies of Liu et al. [11] and Wang et al. [50] revealed same results.

3.4. Temperature effects and thermodynamics analysis

Temperature is also an important environment factor that affects the treatment processes adopting the sorption technique [51,52]. Therefore, temperature effect on the adsorption performance of $FeNi_3$@SiO_2@CuS for MB was examined within a temperature range of 5°C–50°C. Results of removal efficiency vs. contact time are presented in Fig. 5. Notably, the other experimental factors like pH, initial dye concentration, and $FeNi_3$@SiO_2@CuS dose were fixed at 12, 30 mg/L, and 1 g/L, respectively. According to the results gained from equilibrium condition, when the temperature rises from 5°C to 50°C, the percentage removal of MB rises significantly from 44.16% to 96.13%. This can be justified by the increment of solubility ratio of the dye and decrease in the water viscosity with high temperature. Such a process makes the movement of pollutant molecules easier in the solution. Moreover, with the rise of temperature, the surface area of the used adsorbent may increase because of pore size enlargement. Therefore, it is highly probable that active sites collide with adsorbate molecules which, consequently, increase the adsorption efficiency [51–53]. Results also showed that the rise in temperature above 20°C did not significantly increase MB removal efficiency. Thus, the adsorption process can be conducted at room temperature without any need for temperature adjustment.

The results of this experiment are further utilized in the thermodynamic analysis of MB adsorption onto $FeNi_3$@SiO_2@CuS magnetic nanocomposite by applying the Eqs. from (10) to (12). The results of the thermodynamic parameters were tabulated (Table 2). The findings indicated that all the determined $\Delta G°$ values were negative, thus spontaneous and feasible adsorption reaction types affected the interaction system of MB-$FeNi_3$@SiO_2@CuS magnetic nanocomposite couple. While, the positive values of $\Delta H°$ and $\Delta S°$ showed that the MB adsorption type was endothermic, and there was an increase in randomness taking place during the reaction of MB dye with $FeNi_3$@SiO_2@CuS nanoparticles. Moreover, an increase in free energy of the pollutant molecules with a rise in temperature means that the adsorption process will be more preferable in this case. Thus, the $\Delta G° < -20$ kJ/mol and $\Delta H° < 25$ kJ/mol, the process of adsorption is physical [54,55].

3.5. Adsorbent dose effects and isotherm study

Fig. 6 presents the results of effect of $FeNi_3$@SiO_2@CuS dose variation from 0.2 to 2 g/L on the MB removal efficiency,

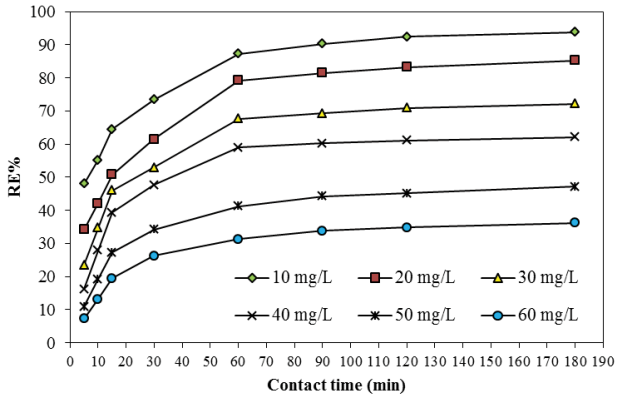

Fig. 4. Plots of the results of the effect of initial MB concentrations on its adsorption process as a function of contact time ($FeNi_3$@SiO_2@CuS dose = 1 g/L, pH = 12, and temperature at ambient condition).

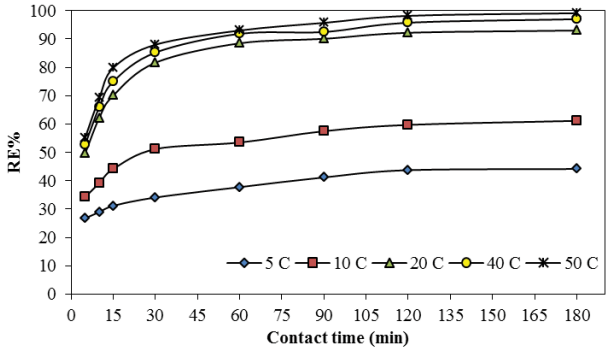

Fig. 5. Plots of the results of the effect of temperature on MB removal efficiency as a function of contact time (pH = 12, initial dye concentration = 30 mg/L, and $FeNi_3$@SiO_2@CuS dose = 1 g/L).

where the solution pH, and initial MB concentration were controlled at values of 12, and 30 mg/L, respectively. This experiment was also conducted by shaking the adsorbent–adsorbate mixtures for a period of 180 min. Clearly, an increase in adsorbent dose was increase in removal efficiency. This increment in due to increase in the values of surface area or number of sorption sites as a result of the increase in the amount of adsorbent particles [56,57]. On another hand, the determined removal efficiencies comparisons at the equilibrium conditions revealed that the addition in the adsorbent quantity in aqueous solution, greater than 1 g/L, has a limited effect of improving MB removal efficiency. The reason behind the appearance of such results is due to the agglomeration tendency of the $FeNi_3$@SiO_2@CuS particles, which was clearly manifested in high doses. As a result, the aggregation of the available sorption sites of the used adsorbent occurred. This findings thoroughly agree with the results obtained from previous studies [22,44,58].

The isotherm study was conducted to get essential information such as the maximum adsorption capacity of the used adsorbent and affinity constants of targeted pollutants. These two parameters are essential for designing adsorption treatment system. Therefore, the experimental data in Fig. 6 (curve of the effects of adsorbent dose at 1 g/L) was modeled on isotherm models (Eqs. (3), (5), and (6)). The nonlinear regression methodology built-in Statistica software was used to make isothermal data comply with theoretical models. Through this methodology, the values of each model's parameters with their corresponding precision coefficients were determined and listed in Table 3. Moreover, Fig. 7 was made in compliance with Table 3 results. Fig. 7 displays the relationship between the experimental isotherm points and theoretical models of MB adsorption onto $FeNi_3$@SiO_2@CuS magnetic nanocomposite. The results obtained demonstrated that the highest R^2 and the lowest RMS values appeared in the case of Langmuir model. These findings demonstrate a single layer sorption process of MB molecules onto a homogeneous surface of $FeNi_3$@SiO_2@CuS nanoparticles [59]. In addition, the value of R_L parameter was 0.16, which reflects desirability of the adsorption process by Langmuir model [60]. Since the n value was set to be >1, a physical adsorption process was involved in the reaction of MB molecules to active sites of $FeNi_3$@SiO_2@CuS [61,62]. This finding is quite consistent with thermodynamic results but contrary to what we have found in the kinetic study that will be shown later. Furthermore, Table 4 showed that the $FeNi_3$@SiO_2@CuS

Table 2
Thermodynamic parameters of MB adsorption onto $FeNi_3$@SiO_2@CuS magnetic nanocomposite

T (K)	$\Delta G°$ (kJ/mol)	$\Delta H°$ (kJ/mol)	$\Delta S°$ (J/mol k)
278	–20.278	0.066	64.970
283	–21.293		
293	–24.184		
313	–26.173		
323	–27.263		

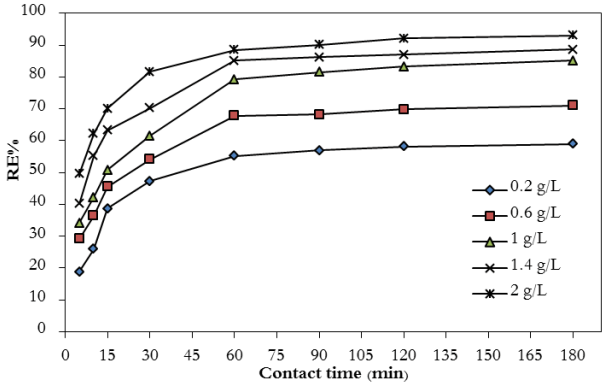

Fig. 6. Plots of the results of the effect of $FeNi_3$@SiO_2@CuS doses effects on MB removal efficiency as a function of contact time (initial dye concentration = 30 mg/L, pH = 12, and temperature at ambient condition).

Table 3
Estimated isotherm and modeling regression parameters of the MB adsorption onto $FeNi_3$@SiO_2@CuS magnetic nanocomposites

Model	Parameter	Value
Langmuir	q_{max} (mg/g)	24.457
	K_L (L/mg)	5.091
	R_L	0.160
	R^2	0.993
	RMSE	1.238
Freundlich	K_f (mg/g)	11.023
	N	4.545
	R^2	0.907
	RMSE	3.129
Temkin	A_T (L/mg)	35.84
	B_T	739.9
	B	3.350
	R^2	0.801
	RMSE	4.532

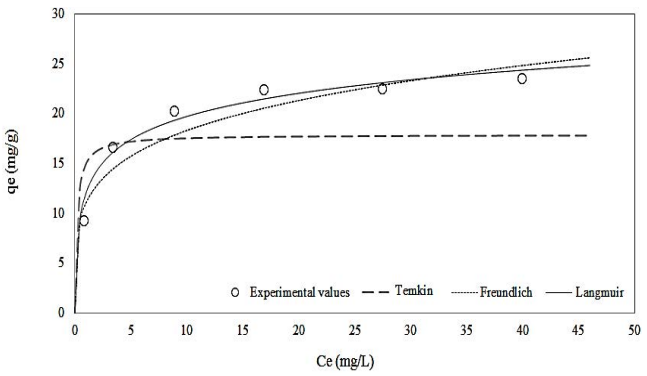

Fig. 7. Plots of the experimental data and theoretical isotherm curves of MB adsorption onto $FeNi_3$@SiO_2@CuS magnetic nanocomposites.

Table 4
Comparison of the uptakes of MB dye by $FeNi_3@SiO_2@CuS$ with other adsorbents

Adsorbent	q_m (mg/g)	pH	Initial MB concentration (mg/L)	Temperature (°C)	Dosage of adsorbent (g/L)	Reference
Rice husk	9.83	–	60–100	30	10	[63]
Pyrolyzed petrified sediment	2.39	7	10–60	30	10	[64]
Coir pith carbon	5.87	–	10–40	35	6	[65]
Activated desert plant	23	6.94	100–1,000	24	4	[66]
Marine seaweed	5.23	7	–	18	–	[67]
Orange peel	18.6	7.2	0–120	–	–	[68]
Banana peel	20.8	7.2	0–120	–	–	[68]
Brown marine macroalga	95.45	–	20–320	–	1	[69]
Modified pine nut shells	39.73	5.9	–	–	–	[70]
Arginine modified activated carbon	219.9	8	–	25	–	[71]
Fe_3O_4@AMCA-MIL-53(AI)	318.36	8.9	25–400	25	20 mg	[72]
$FeNi_3@SiO_2@CuS$	24.45	12	30	25	1	This study

exhibited an excellent adsorption capacity for MB dye, compared with other adsorbents used for the same purpose.

3.6. Adsorption kinetics

Understanding kinetics of adsorption process is very important point in the designing of treatment system. It is because kinetics studies of the adsorption treatment processes provide important information on reaction mechanism that occurs (i.e., chemical, physical type). In addition, it might be used to specify the dominant rate-limiting step of the removal process of pollutant and mass transfer parameter [30,73]. As a result, the design parameters and operation aspects linked to adsorption process are dependable, based on the kinetic study. In this direction, kinetics data should be properly modeled to cope with the relevant models of kinetics reaction to secure a representative model for the adsorption kinetics process. The three kinetic models (previously illustrated in Eqs. (7)–(9) in the current study) are modeled, using the data of experiment of the effect of initial dye concentrations at 30 mg/L (Fig. 4). Parameter results of each model are listed in Table 5. Fig. 8 also graphically shows the results of the application of the kinetic models for the modeling of kinetic data of MB adsorption onto $FeNi_3@SiO_2@CuS$ magnetic nanocomposites. The results indicated that, the second-order model was the best one to fit experimental data in which the highest R^2 and the lowest RMSE values were determined. In addition, this model exhibited uptake value (9.80 mg/g), very close to the real one (10.04 mg/m). Because of the assumption of kinetic mechanism of the second-order model that is based on chemical adsorption in addition to the thermodynamic and isotherm studies which exhibited physical adsorption, one can deduce that the major reaction of MB to the surface of the synthesized $FeNi_3@SiO_2@CuS$ magnetic nanocomposites that occurs through both chemisorption and physical processes [74,75].

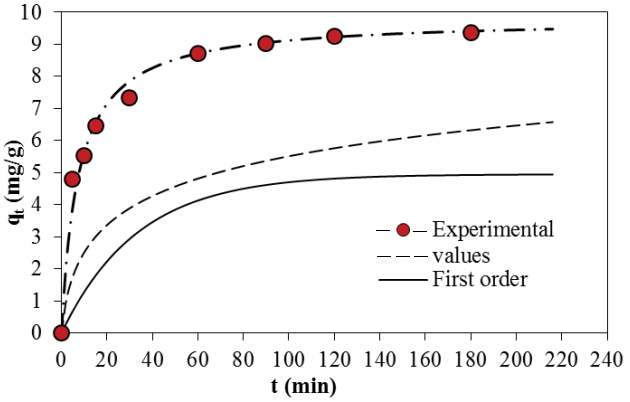

Fig. 8. Plots of the experimental and theoretical kinetic values of MB adsorption onto $FeNi_3@SiO_2@CuS$ magnetic nanocomposites.

Table 5
Kinetics parameters and the R^2 and RMSE values of MB adsorption onto $FeNi_3@SiO_2@CuS$ magnetic nanocomposites ($q_{e,cal}$ and $q_{e,exp}$ refer to MB uptakes that were calculated and determined experimentally, respectively)

Model	Parameters	Values
$q_{e,exp}$ (mg/g)		10.04
Pseudo-first-order	$q_{e,cal}$ (mg/g)	4.950
	k_1 (1/min)	0.030
	R^2	0.990
	RMSE	3.12
Pseudo-second-order	$q_{e,cal}$ (mg/g)	9.800
	k_2 (1/min)	0.0137
	R^2	0.999
	RMSE	0.250
Elovich	α	0.706
	β	0.714
	R^2	0.978
	RMSE	2.400

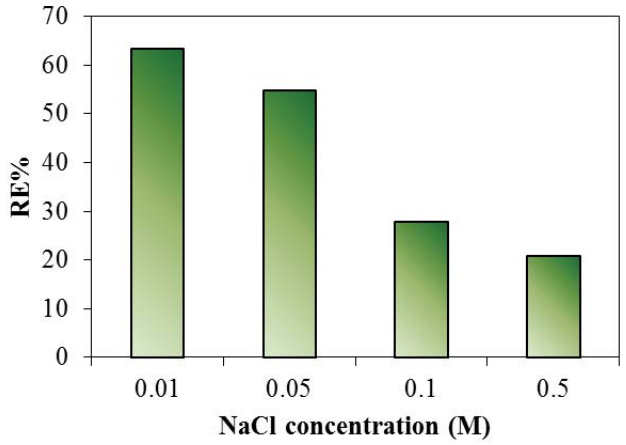

Fig. 9. Effect of NaCl concentration on MB adsorption (initial dye concentration = 20 mg/L, pH = 12, $FeNi_3$@SiO_2@CuS dose = 2 g/L, and temperature at ambient condition).

3.7. Effect of the presence of NaCl

The results of the effect of the NaCl on the adsorption process are displayed in Fig. 9. The increase in NaCl concentration had significantly decreased the removal efficiency. This is because NaCl particles c with MB molecules on the same adsorption sites, thus the removal efficiency of this dye dramatically decreased.

4. Conclusion

The present study concluded that $FeNi_3$@SiO_2@CuS magnetic nanocomposites have the high adsorbent capacity for the MB molecules in aqueous solution. The analysis of TEM, FESEM results showed that the average size of the synthesized nano-adsorbent was determined to be between 24 and 63. The hysteresis loops analysis using the VSM technique indicates that the synthesized adsorbent has a paramagnetic property might be separated by an external magnetic field. According to findings of the current study, the highest uptake of the synthesized nanocomposite for MB was found to be 24.457 mg/g according to results of the best fit model of Langmuir. This uptake was determined at the optimized conditions: pH = 12, equilibration contact time = 180 min, initial MB concentration = 20 mg/L, and $FeNi_3$@SiO_2@CuS dose = 2 g/L. The kinetic adsorption adopted the pseudo-second-order model. Spontaneous and endothermic adsorption was characteristics of MB adsorption onto $FeNi_3$@SiO_2@CuS, as induced by the results of effect of temperature and thermodynamics analyses. Finally, the findings revealed that the synthesized $FeNi_3$@SiO_2@CuS has a high potential value which can be applied in full-scale as an efficient adsorbent over adsorption treatment process of MB contaminant.

Acknowledgments

The researchers are greatly indebted to Payame Noor University of Tehran for the technical support given to this research. They also would like to extend their thanks to Isra University, and also to Isam Kayed's center for translation, courses, and training for the invaluable help it offered with regard to language editing. The Ethics Committee of Birjand University of Medical Sciences approved the study with the ethical code of IR.BUMS.REC.1399.151.

References

[1] I. Bashir, F.A. Lone, R.A. Bhat, S.A. Mir, Z.A. Dar, S.A. Dar, Concerns and Threats of Contamination on Aquatic Ecosystems, K. Hakeem, R. Bhat, H. Qadri, Eds., Bioremediation and Biotechnology, Springer, Cham, 2020, pp. 1–26.
[2] N. Ferronato, V. Torretta, Waste mismanagement in developing countries: a review of global issues, Int. J. Environ. Res. Public Health, 16 (2019) 1060, doi: 10.3390/ijerph16061060.
[3] K.S. Kuppusamy, M. Priya, Biologial treatment of AZO dyes and textile industry effluent by newly isolated white ROT fungi *Schizophyllum* commune and *Lenzites eximia*, Int. J. Environ. Sci., 2 (2012) 1938–1947.
[4] P. Malik, Dye removal from wastewater using activated carbon developed from sawdust: adsorption equilibrium and kinetics, J. Hazard. Mater., 113 (2004) 81–88.
[5] B. Zargar, H. Parham, M. Rezazade, Fast removal and recovery of methylene blue by activated carbon modified with magnetic iron oxide nanoparticles, J. Chin. Chem. Soc., 58 (2011) 694–699.
[6] M. Vinuth, H.S.B. Naik, B.M. Vinoda, H. Gururaj, N. Thomas, G. Arunkumar, Enhanced removal of methylene blue dye in aqueous solution using eco-friendly Fe(III)–montmorillonite, Mater. Today: Proc., 4 (2017) 424–433.
[7] J. Zhang, M.S. Azam, C. Shi, J. Huang, B. Yan, Q. Liu, H. Zeng, Poly(acrylic acid) functionalized magnetic graphene oxide nanocomposite for removal of methylene blue, RSC Adv., 5 (2015) 32272–32282.
[8] M. Salehi, H. Hashemipour, M. Mirzaee, Experimental study of influencing factors and kinetics in catalytic removal of methylene blue with TiO_2 nanopowder, Am. J. Environ. Eng., 2 (2012) 1–7.
[9] D. Balarak, T.J. Al-Musawi, I.A. Mohammed, H. Abasizadeh, The eradication of reactive black 5 dye liquid wastes using *Azolla filiculoides* aquatic fern as a good and an economical biosorption agent, SN Appl. Sci., 2 (2020) 1015, doi: 10.1007/s42452-020-2841-x.
[10] R. Liu, P. Lv, H. Fu, R. Lu, X. Wu, Y. Lu, Removal performance of methyl blue onto magnetic $MgFe_2O_4$ nanoparticles prepared via the rapid combustion process, J. Nanosci. Nanotechnol., 17 (2017) 4755–4762.
[11] H.M. Zwain, M. Vakili, I. Dahlan, Waste material adsorbents for zinc removal from wastewater: a comprehensive review, Int. J. Chem. Eng., 2014 (2014) 347912, doi: 10.1155/2014/347912.
[12] S. Das, J. Chakraborty, S. Chatterjee, H. Kumar, Prospects of biosynthesized nanomaterials for the remediation of organic and inorganic environmental contaminants, Environ. Sci. Nano, 5 (2018) 2784–2808.
[13] N. Nasseh, F.S. Arghavan, S. Rodriguez-Couto, A. Hossein Panahi, Synthesis of $FeNi_3$/SiO_2/CuS magnetic nano-composite as a novel adsorbent for Congo Red dye removal, Int. J. Environ. Anal. Chem., (2020) 1–21, doi: 10.1080/03067319.2020.1754810 (in Press).
[14] T. Tatarchuk, N. Paliychuk, R. Babu Bitra, A. Shyichuk, M. Naushad, I. Mironyuk, D. Ziolkovska, Adsorptive removal of toxic Methylene Blue and Acid Orange 7 dyes from aqueous medium using cobalt-zinc ferrite nanoadsorbents, Desal. Water Treat., 150 (2019) 374–385.
[15] J. Wu, J. Bai, Z. Wang, Z. Liu, Y. Mao, B. Liu, X. Zhu, UV-assisted nitrogen-doped reduced graphene oxide/Fe_3O_4 composite activated peroxodisulfate degradation of norfloxacin, Environ. Technol., (2020) 1–12, doi: 10.1080/09593330.2020.1779353 (in Press).
[16] S.S. Banerjee, D.-H. Chen, Fast removal of copper ions by gum arabic modified magnetic nano-adsorbent, J. Hazard. Mater., 147 (2007) 792–799.
[17] M. Khodadadi, M. Ehrampoush, M. Ghaneian, A. Allahresani, A. Mahvi, Synthesis and characterizations of $FeNi_3$@SiO_2@

TiO_2 nanocomposite and its application in photo-catalytic degradation of tetracycline in simulated wastewater, J. Mol. Liq., 255 (2018) 224–232.
[18] A.A. Alqadami, M. Naushad, Z.A. Alothman, A.A. Ghfar, Novel metal–organic framework (MOF) based composite material for the sequestration of U(VI) and Th(IV) metal ions from aqueous environment, ACS Appl. Mater. Interface, 9 (2017) 36026–36037.
[19] A.A. Alqadami, M. Naushad, M.A. Abdalla, M.R. Khan, Z.A. Alothman, Adsorptive removal of toxic dye using Fe_3O_4–TSC nanocomposite: equilibrium, kinetic, and thermodynamic studies, J. Chem. Eng. Data, 61 (2016) 3806–3813.
[20] N. Nasseh, L. Taghavi, B. Barikbin, M.A. Nasseri, Synthesis and characterizations of a novel $FeNi_3/SiO_2/CuS$ magnetic nanocomposite for photocatalytic degradation of tetracycline in simulated wastewater, J. Cleaner Prod., 179 (2018) 42–54.
[21] M.A. Nasseri, S.M. Sadeghzadeh, A highly active $FeNi_3$–SiO_2 magnetic nanoparticles catalyst for the preparation of 4H-benzo [b] pyrans and spirooxindoles under mild conditions, J. Iran. Chem. Soc., 10 (2013) 1047–1056.
[22] N. Nasseh, L. Taghavi, B. Barikbin, M.A. Nasseri, A. Allahresani, $FeNi_3/SiO_2$ magnetic nanocomposite as an efficient and recyclable heterogeneous Fenton-like catalyst for the oxidation of metronidazole in neutral environments: adsorption and degradation studies, Composites, Part B, 166 (2019) 328–340.
[23] T. Etemadinia, A. Allahrasani, B. Barikbin, $ZnFe_2O_4@SiO_2@$ Tragacanth gum nanocomposite: synthesis and its application for the removal of methylene blue dye from aqueous solution, Polym. Bull., 76 (2019) 6089–6109.
[24] S.M. Seyed Arabi, R.S. Lalehloo, M.R.T.B. Olyai, G.A.M. Ali, H. Sadegh, Removal of congo red azo dye from aqueous solution by ZnO nanoparticles loaded on multiwall carbon nanotubes, Physica E, 106 (2019) 150–155.
[25] A.C. Martins, O. Pezoti, A.L. Cazetta, K.C. Bedin, D.A. Yamazaki, G.F. Bandoch, T. Asefa, J.V. Visentainer, V.C. Almeida, Removal of tetracycline by NaOH-activated carbon produced from macadamia nut shells: kinetic and equilibrium studies, Chem. Eng. J., 260 (2015) 291–299.
[26] G. Moussavi, R. Khosravi, The removal of cationic dyes from aqueous solutions by adsorption onto pistachio hull waste, Chem. Eng. Res. Des., 89 (2011) 2182–2189.
[27] V.K. Gupta, S. Agarwal, H. Sadegh, G.A.M. Ali, A.K. Bharti, A.S. Hamdy Makhlouf, Facile route synthesis of novel graphene oxide-β-cyclodextrin nanocomposite and its application as adsorbent for removal of toxic bisphenol A from the aqueous phase, J. Mol. Liq., 237 (2017) 466–472.
[28] M. Kamranifar, M. Khodadadi, V. Samiei, B. Dehdashti, M.N. Sepehr, L. Rafati, N. Nasseh, Comparison the removal of reactive red 195 dye using powder and ash of barberry stem as a low cost adsorbent from aqueous solutions: isotherm and kinetic study, J. Mol. Liq., 255 (2018) 572–577.
[29] G. Moussavi, R. Khosravi, Removal of cyanide from wastewater by adsorption onto pistachio hull wastes: parametric experiments, kinetics and equilibrium analysis, J. Hazard. Mater., 183 (2010) 724–730.
[30] Y.S. Ho, G. McKay, Pseudo-second order model for sorption processes, Process Biochem., 34 (1999) 451–465.
[31] S. Agarwal, H. Sadegh, M. Monajjemi, A.S. Hamdy, G.A.M. Ali, A.O.H. Memar, R. Shahryari-Ghoshekandi, I. Tyagi, V.K. Gupta, Efficient removal of toxic bromothymol blue and methylene blue from wastewater by polyvinyl alcohol, J. Mol. Liq., 218 (2016) 191–197.
[32] Y. Khambhaty, K. Mody, S. Basha, B. Jha, Kinetics, equilibrium and thermodynamic studies on biosorption of hexavalent chromium by dead fungal biomass of marine *Aspergillus niger*, Chem. Eng. J., 145 (2009) 489–495.
[33] H. Sadegh, G. Ali, Z. Khalifehlou, M. Nadagouda, Adsorption of ammonium ions onto multi-walled carbon nanotubes, Stud. Univ. Babes-Bolyai Chem., 62 (2017) 233–245.
[34] J.C. Morris, W.J. Weber Jr, Removal of Biologically-Resistant Pollutants from Wastewaters by Adsorption, Advances in Water Pollution Research, Vol. 2, Elsevier, Oxford, 1964, pp. 231–266.
[35] X. Li, Y. Liu, C. Zhang, T. Wen, L. Zhuang, X. Wang, G. Song, D. Chen, Y. Ai, T. Hayat, X. Wang, Porous Fe_2O_3 microcubes derived from metal organic frameworks for efficient elimination of organic pollutants and heavy metal ions, Chem. Eng. J., 336 (2018) 241–252.
[36] S. Karthikeyan, V. Gupta, R. Boopathy, A. Titus, G. Sekaran, A new approach for the degradation of high concentration of aromatic amine by heterocatalytic Fenton oxidation: kinetic and spectroscopic studies, J. Mol. Liq., 173 (2012) 153–163.
[37] Y. Jia, Y. Zhang, J. Fu, L. Yuan, Z. Li, C. Liu, D. Zhao, X. Wang, A novel magnetic biochar/MgFe-layered double hydroxides composite removing Pb^{2+} from aqueous solution: isotherms, kinetics and thermodynamics, Colloids Surf., A, 567 (2019) 278–287.
[38] N. Nasseh, T.J. Al-Musawi, M.R. Miri, S. Rodriguez-Couto, A. Hossein Panahi, A comprehensive study on the application of $FeNi_3@SiO_2@ZnO$ magnetic nanocomposites as a novel photo-catalyst for degradation of tamoxifen in the presence of simulated sunlight, Environ. Pollut., 261 (2020) 114127, doi: 10.1016/j.envpol.2020.114127.
[39] M. Naushad, G. Sharma, Z. Alothman, Photodegradation of toxic dye using Gum Arabic-crosslinked-poly(acrylamide)/$Ni(OH)_2$/FeOOH nanocomposites hydrogel, J. Cleaner Prod., 241 (2019) 118263, doi: 10.1016/j.jclepro.2019.118263.
[40] X. Ding, Y. Huang, J. Wang, H. Wu, P. Liu, Excellent electromagnetic wave absorption property of quaternary composites consisting of reduced graphene oxide, polyaniline and $FeNi_3@SiO_2$ nanoparticles, Appl. Surf. Sci., 357 (2015) 908–914.
[41] N. Nasseh, F.S. Arghavan, S. Rodriguez-Couto, A. Hossein Panahi, M. Esmati, T.J. A-Musawi, Preparation of activated carbon@ZnO composite and its application as a novel catalyst in catalytic ozonation process for metronidazole degradation, Adv. Powder. Technol., 31 (2020) 875–885.
[42] Z.L. Yaneva, N.V. Georgieva, Insights into Congo Red adsorption on agro-industrial materials - spectral, equilibrium, kinetic, thermodynamic, dynamic and desorption studies, a review, Int. Rev. Chem. Eng., 4 (2012) 127–146.
[43] Y. Sun, H. Li, G. Li, B. Gao, Q. Yue, X. Li, Characterization and ciprofloxacin adsorption properties of activated carbons prepared from biomass wastes by H_3PO_4 activation, Bioresour. Technol., 217 (2016) 239–244.
[44] J.R. Kim, B. Santiano, H. Kim, E. Kan, Heterogeneous oxidation of methylene blue with surface-modified iron-amended activated carbon, Am. J. Anal. Chem., 4 (2013) 115–122.
[45] A. Seidmohammadi, G. Asgari, M. Leili, A. Dargahi, A. Mobarakian, Effectiveness of quercus branti activated carbon in removal of methylene blue from aqueous solutions, Arch. Hyg. Sci., 4 (2015) 217–225.
[46] R. Coşkun, A. Yıldız, A. Delibaş, Removal of methylene blue using fast sucking adsorbent, J. Mater. Environ. Sci., 8 (2017) 398–409.
[47] S. Wang, Q. Gao, W. Luo, J. Xu, C. Zhou, H. Xia, Removal of methyl blue from aqueous solution by magnetic carbon nanotube, Water Sci. Technol., 68 (2013) 665–673.
[48] J. Jang, H. Lim, Characterization and analytical application of surface modified magnetic nanoparticles, Microchem. J., 94 (2010) 148–158.
[49] R. Sahraei, Z.S. Pour, M. Ghaemy, Novel magnetic bio-sorbent hydrogel beads based on modified gum tragacanth/graphene oxide: removal of heavy metals and dyes from water, J. Cleaner Prod., 142 (2017) 2973–2984.
[50] A. Wang, W. Wang, Gum-g-Copolymers: Synthesis, Properties, and Applications, S. Kalia, M.W. Sabaa, Eds., Polysaccharide Based Graft Copolymers, Springer, Berlin, Heidelberg, 2013, pp. 149–203.
[51] B. Mudyawabikwa, H.H. Mungondori, L. Tichagwa, D.M. Katwire, Methylene blue removal using a low-cost activated carbon adsorbent from tobacco stems: kinetic and equilibrium studies, Water Sci. Technol., 75 (2017) 2390–2402.
[52] S. Cheng, L. Zhang, H. Xia, J. Peng, J. Shu, C. Li, X. Jiang, Q. Zhang, Adsorption behavior of methylene blue onto waste-derived adsorbent and exhaust gases recycling, RSC Adv., 7 (2017) 27331–27341.
[53] S. Hong, C. Wen, J. He, F. Gan, Y.-S. Ho, Adsorption thermodynamics of Methylene Blue onto bentonite, J. Hazard. Mater., 167 (2009) 630–633.

[54] N.G. Rincón-Silva, J.C. Moreno-Piraján, L.G. Giraldo, Thermodynamic study of adsorption of phenol, 4-chlorophenol, and 4-nitrophenol on activated carbon obtained from eucalyptus seed, J. Chem., 2015 (2015) 569403, doi: 10.1155/2015/569403.
[55] R. Tang, C. Dai, C. Li, W. Liu, S. Gao, C. Wang, Removal of methylene blue from aqueous solution using agricultural residue walnut shell: equilibrium, kinetic, and thermodynamic studies, J. Chem., 2017 (2017) 8404965, doi: 10.1155/2017/8404965.
[56] G. Asgari, A. Dargahi, S.A. Mobarakian, Equilibrium and synthetic equations for index removal of methylene blue using activated carbon from oak fruit bark, J. Mazandaran Univ. Med. Sci., 24 (2015) 172–187.
[57] M. Leili, B. Ramavandi, The efficiency evaluation of activated carbon prepared from date stones for removal of methylene blue dye from aqueous solutions, J. Sabzevar Univ. Med. Sci., 21 (2014) 502–513.
[58] V.K. Gupta, D. Pathania, N. Kothiyal, G. Sharma, Polyaniline zirconium(IV) silicophosphate nanocomposite for remediation of methylene blue dye from waste water, J. Mol. Liq., 190 (2014) 139–145.
[59] H.H. Abdel Ghafar, G.A.M. Ali, O.A. Fouad, S.A. Makhlouf, Enhancement of adsorption efficiency of methylene blue on Co_3O_4/SiO_2 nanocomposite, Desal. Water Treat., 53 (2015) 2980–2989.
[60] Z. Mohammadi, M. Sharif Zak, H. Majdi, K. Seidi, M. Barati, A. Akbarzadeh, A.M. Latifi, The effect of chrysin-loaded nanofiber on wound healing process in male rat, Chem. Biol. Drug Des., 90 (2017) 1106–1114.
[61] A.M. Aljeboree, A.N. Alshirifi, A.F. Alkaim, Kinetics and equilibrium study for the adsorption of textile dyes on coconut shell activated carbon, Arabian J. Chem., 10 (2017) S3381–S3393.
[62] P.S. Kumar, S. Ramalingam, C. Senthamarai, M. Niranjanaa, P. Vijayalakshmi, S. Sivanesan, Adsorption of dye from aqueous solution by cashew nut shell: studies on equilibrium isotherm, kinetics and thermodynamics of interactions, Desalination, 261 (2010) 52–60.
[63] Y.C. Sharma, Uma, Optimization of parameters for adsorption of methylene blue on a low-cost activated carbon, J. Chem. Eng. Data, 55 (2010) 435–439.
[64] A.Z. Aroguz, J. Gulen, R.H. Evers, Adsorption of methylene blue from aqueous solution on pyrolyzed petrified sediment, Bioresour. Technol., 99 (2008) 1503–1508.
[65] D. Kavitha, C. Namasivayam, Experimental and kinetic studies on methylene blue adsorption by coir pith carbon, Bioresour. Technol., 98 (2007) 14–21.
[66] B. Bestani, N. Benderdouche, B. Benstaali, M. Belhakem, A. Addou, Methylene blue and iodine adsorption onto an activated desert plant, Bioresour. Technol., 99 (2008) 8441–8444.
[67] S. Cengiz, L. Cavas, Removal of methylene blue by invasive marine seaweed: *Caulerpa racemosa* var. cylindracea, Bioresour. Technol., 99 (2008) 2357–2363.
[68] G. Annadurai, R.-S. Juang, D.-J. Lee, Use of cellulose-based wastes for adsorption of dyes from aqueous solutions, J. Hazard. Mater., 92 (2002) 263–274.
[69] E. Daneshvar, A. Vazirzadeh, A. Niazi, M. Kousha, M. Naushad, A. Bhatnagar, Desorption of Methylene blue dye from brown macroalga: effects of operating parameters, isotherm study and kinetic modeling, J. Cleaner Prod., 152 (2017) 443–453.
[70] M. Naushad, M. Ali Khan, Z. Abdullah Alothman, M. Rizwan Khan, M. Kumar, Adsorption of methylene blue on chemically modified pine nut shells in single and binary systems: isotherms, kinetics, and thermodynamic studies, Desal. Water Treat., 57 (2016) 15848–15861.
[71] M. Naushad, A.A. Alqadami, Z.A. Alothman, I.H. Alsohaimi, M.S. Algamdi, A.M. Aldawsari, Adsorption kinetics, isotherm and reusability studies for the removal of cationic dye from aqueous medium using arginine modified activated carbon, J. Mol. Liq., 293 (2019) 111442, doi: 10.1016/j.molliq.2019.111442.
[72] A.A. Alqadami, M. Naushad, Z.A. Alothman, T. Ahamad, Adsorptive performance of MOF nanocomposite for methylene blue and malachite green dyes: kinetics, isotherm and mechanism, J. Environ. Manage., 223 (2018) 29–36.
[73] F. Brouers, T.J. Al-Musawi, Brouers-Sotolongo fractal kinetics versus fractional derivative kinetics: a new strategy to analyze the pollutants sorption kinetics in porous materials, J. Hazard. Mater., 350 (2018) 162–168.
[74] H. Sadegh, G.A.M. Ali, S. Agarwal, V.K. Gupta, Surface modification of MWCNTs with carboxylic-to-amine and their superb adsorption performance, Int. J. Environ. Res., 13 (2019) 523–531.
[75] B. Maazinejad, O. Mohammadnia, G.A.M. Ali, A.S.H. Makhlouf, M.N. Nadagouda, M. Sillanpää, A.M. Asiri, S. Agarwal, V.K. Gupta, H. Sadegh, Taguchi L9 (34) orthogonal array study based on methylene blue removal by single-walled carbon nanotubes-amine: adsorption optimization using the experimental design method, kinetics, equilibrium and thermodynamics, J. Mol. Liq., 298 (2020) 112001, doi: 10.1016/j.molliq.2019.112001.